Phase-field approach to implicit solvation of biomolecules with Coulomb-field approximation

Yanxiang Zhao, Yuen-Yick Kwan, Jianwei Che, Bo Li, and J. Andrew McCammon

---

Articles you may be interested in

A self-consistent phase-field approach to implicit solvation of charged molecules with Poisson–Boltzmann electrostatics
J. Chem. Phys. **143**, 243110 (2015); 10.1063/1.4932336

Bounding the electrostatic free energies associated with linear continuum models of molecular solvation
J. Chem. Phys. **130**, 104108 (2009); 10.1063/1.3081148

Estimation of absolute solvent and solvation shell entropies via permutation reduction
J. Chem. Phys. **126**, 014102 (2007); 10.1063/1.2400220

Analytical electrostatics for biomolecules: Beyond the generalized   Born approximation
J. Chem. Phys. **124**, 124902 (2006); 10.1063/1.2177251

Continuum description of solvent dielectrics in molecular-dynamics simulations of proteins
J. Chem. Phys. **118**, 2039 (2003); 10.1063/1.1532730

Phase-field approach to implicit solvation of biomolecules with Coulomb-field approximation

Yanxiang Zhao,[1,2,a)] Yuen-Yick Kwan,[1,2,b)] Jianwei Che,[3,c)] Bo Li,[1,2,d)] and J. Andrew McCammon[2,4,e)]

[1]*Department of Mathematics, University of California, San Diego, 9500 Gilman Drive, Mail code: 0112, La Jolla, California 92093-0112, USA*
[2]*Center for Theoretical Biological Physics, University of California, San Diego, MC 0374, 9500 Gilman Drive, La Jolla, California 92093-0374, USA*
[3]*The Genomics Institute of the Novartis Research Foundation, 10675 John Jay Hopkins Drive, San Diego, California 92121, USA*
[4]*Department of Chemistry and Biochemistry, Department of Pharmacology, Howard Hughes Medical Institute, University of California, San Diego, La Jolla, California 92093, USA*

A phase-field variational implicit-solvent approach is developed for the solvation of charged molecules. The starting point of such an approach is the representation of a solute-solvent interface by a phase field that takes one value in the solute region and another in the solvent region, with a smooth transition from one to the other on a small transition layer. The minimization of an effective free-energy functional of all possible phase fields determines the equilibrium conformations and free energies of an underlying molecular system. All the surface energy, the solute-solvent van der Waals interaction, and the electrostatic interaction are coupled together self-consistently through a phase field. The surface energy results from the minimization of a double-well potential and the gradient of a field. The electrostatic interaction is described by the Coulomb-field approximation. Accurate and efficient methods are designed and implemented to numerically relax an underlying charged molecular system. Applications to single ions, a two-plate system, and a two-domain protein reveal that the new theory and methods can capture capillary evaporation in hydrophobic confinement and corresponding multiple equilibrium states as found in molecular dynamics simulations. Comparisons of the phase-field and the original sharp-interface variational approaches are discussed. © 2013 AIP Publishing LLC. [http://dx.doi.org/10.1063/1.4812839]

I. INTRODUCTION

The structure, dynamics, and function of biomolecular systems are crucially influenced by the interaction between the biomolecules and their aqueous environment. Such interactions can be described efficiently by implicit-solvent models[1–4] in which the solvent molecules and ions are treated implicitly and their effects are coarse-grained. These models are complementary to the more accurate but computationally expensive explicit-solvent models, such as molecular dynamics and Monte Carlo simulations, which often provide sampled statistical information rather than direct descriptions of thermodynamics.

A large class of existing implicit-solvent models is based on various kinds of predefined solute-solvent interfaces, such as the van der Waals surface (vdWS), solvent-excluded surface (SES), or solvent-accessible surface (SAS).[5–9] In these models, the solvation free energy is approximated by the sum of two parts. One is the interfacial energy which is often taken to be proportional to the surface area. The other is the electrostatic free energy which is often determined by the Poisson-Boltzmann[10–14] or generalized Born[15–18] theory in which a vdWS, SES, or SAS is used as a dielectric boundary. While such fixed-surface, implicit-solvent approaches have been successful in many cases, their accuracy and general applicability are still questionable. It is believed that one of the main issues here is the decoupling of surface energy, dispersion, and electrostatic interaction. Moreover, an *ad hoc* definition of vdWS, SAS, or SES can often lead to inaccurate free-energy calculations. It is additionally well established by now that cavitation free energies do not scale with surface area for high curvatures,[19–22] a fact of critical importance in the implicit-solvent modeling of hydrophobic interactions at molecular scales.[23–27]

In recent years, a new class of surface based, implicit-solvent models—the variational implicit-solvent model (VISM)—has been developed.[28,29] Coupled with the robust level-set numerical method, such models allow an efficient and quantitative description of molecular solvation.[30–36] Central in the VISM is a mean-field free-energy functional of all possible solute-solvent interfaces, or dielectric boundaries, that separate the continuum solvent from all solute atoms. In a simple setting, such a free-energy functional consists of surface energy, solute-solvent van der Waals interaction

a)Electronic mail: y1zhao@ucsd.edu
b)Electronic mail: yykwan@ucsd.edu
c)Electronic mail: jche@gnf.org
d)Electronic mail: bli@math.ucsd.edu
e)Electronic mail: jmccammon@ucsd.edu

energy, and continuum electrostatic free energy. The minimization of the functional determines the solvation free energies and stable equilibrium solute-solvent interfaces. Extensive level-set numerical results with comparison with experiment and molecular dynamics simulations have demonstrated the success of this new approach to the solvation of molecular systems in describing the hydrophobic interaction, capturing multiple equilibrium states of hydration, and providing good estimates of solvation free energies.[30,32,33,35] In general, a stable equilibrium solute-solvent interface determined by the level-set VISM can be quite different from a vdWS, SES, or SAS, particularly when it comes to the description of hydrophobic interactions.[20,27,37] Perhaps the most significant feature of VISM is that its free-energy functional exhibits a complex energy landscape with multiple local minima corresponding to different equilibrium states.

In this work, we develop a phase-field VISM, often abbreviated as P-VISM, as an alternative to the original VISM that uses a sharp-interface formulation to the solvation of charged molecules. The phase-field theory and method have been widely used in studying interface problems arising in many scientific areas such as materials physics, complex fluids, and biomembranes, cf., e.g., Refs. [38–49] and the references therein. In a phase-field model, an interface separating two regions is represented by a continuous function that takes values close to one constant in one of the regions and another constant in the other region, but smoothly changes its values from one of the constants to another in a thin transition region. (We choose these constant values to be 0 and 1, respectively.) It is in this way that a phase field defines a diffuse interface. Both the sharp-interface and the diffuse-interface approaches have their own advantages and disadvantages. For instance, in phase-field computations, explicit tracking of moving boundaries is avoided. But an extra fit-parameter, a numerical constant that characterizes the size of transition layer, is introduced. We have two particular reasons to develop a phase-field VISM. First, existing studies have shown that interfacial fluctuations can be described in a phase-field approach.[50–52] Such fluctuations are particularly crucial in the transition of one equilibrium conformation to another in a biomolecular system. It seems, however, the direct inclusion of fluctuations in a sharp-interface model is not straightforward. Second, a phase field can describe well the transition from solute to solvent. With some modeling refinement, such a field can likely be used to describe the hydration shell in the framework of implicit-solvent modeling.

Fundamental in our phase-field variational approach to the implicit solvation of charged molecules is a mean-field free-energy functional of all possible phase fields. Minimization of the free-energy functional determines the minimum free energies as well as the stable equilibrium conformations of an underlying biomolecular system. In our previous work,[53] we proposed such free-energy functionals and proved mathematically that they "converge" to the sharp-interface VISM functional. As in the original VISM, our phase-field free-energy functional couples all the surface energy, the solute-solvent van der Waals interactions, and the electrostatic interactions through a phase field. The surface energy is taken to be proportional to the surface area. In the free-energy functional of phase field $\phi = \phi(\mathbf{x})$, the approximation of the surface area is given by

$$\int \left[\frac{\xi}{2} |\nabla \phi|^2 + \frac{1}{\xi} W(\phi) \right] d\mathbf{x},$$

where $\xi > 0$ is a small parameter characterizing the width of transition layer and W is a properly chosen double-well potential. If a phase field ϕ has a low free energy, then the W-term forces the phase field ϕ to be close to the two wells of W, partitioning the underlying solvation region into the solute and solvent regions, while the gradient term penalizes such partitioning. As the parameter ξ becomes smaller and smaller, the transition layer characterized by a phase field becomes thinner and thinner, and the corresponding integral value approaches the interfacial area.[53–55] This well established mathematical theory is the foundation of the phase-field approach. As in the sharp-interface version of VISM, we model the solute-solvent van der Waals interaction by the sum of Lennard-Jones potentials of pair-wise interactions between all the solute particles and solvent molecules that are now treated as a continuum. We also describe the electrostatic part of the solvation free energy by the Coulomb-field approximation that we have developed recently.[35,36]

Much of our work is devoted to the design, implementation, and test of accurate and efficient numerical methods for solving the gradient-flow (i.e., the steepest descent) partial differential equations of relaxing our phase-field free-energy functional. We use a semi-implicit scheme for the time discretization. In each time step, we use the spectral method for the spatial discretization and use the fast Fourier transformation to solve the linear system of equations of the discretization.

We also apply our theory and method to several charged molecular systems of different complexity. First, we consider the hydration of some single ions and compare our phase-field calculations with experiment. Our second system consists of two hydrophobic plates for which we calculate the potential of mean force with the plate-plate distance as the reaction coordinate. The last system is the two-domain protein biphenyl-2,3-diol-1,2-dioxygenase (BphC). For this system, we compare our results with those of molecular dynamics simulations[26] and the sharp-interface variational implicit-solvent modeling.[36]

We notice that several related issues, such as coupling the solvent boundary to the optimization of overall energy, the curvature effect to surface energy, and dewetting transition, have been discussed in literature.[25,56–58] Other related models and methods have also been proposed.[4,59–62] A similar solvation model is proposed in Ref. [62], where the surface energy is approximated by the integral of $\gamma |\nabla S|$ with γ being the surface energy density and S a field similar to our ϕ. However, there are no terms in the total free-energy functional G_{total} (cf. Eq. (7) in Ref. [62]) that can keep the field S to be close to two distinct values so that the system region can be partitioned into the solute and solvent regions by the field S. Unless an equilibrium boundary or field S is *a priori* known, the minimization of the total free-energy functional will smooth out the field S to reduce the surface energy.

The rest of the paper is organized as follows: In Sec. II, we present our phase-field VISM for molecular solvation. In Sec. III, we describe our computational methods for solving the partial differential equation of the gradient-flow of the phase-field free-energy functional. In Sec. IV, we apply our theory and methods to the solvation of single ions, a two-plate system, and the two-domain protein BphC. Finally, in Sec. V, we draw conclusions of our studies.

II. THEORY

We consider a system of molecular solvation that occupies a finite region Ω in $\mathbb{R}^3$. The system consists of solute atoms located at $\mathbf{x}_1, \ldots, \mathbf{x}_N$ in Ω together with the solvent that is treated as a continuum with a uniform density ρ_w. Let $\xi > 0$ be a small parameter with units in length. In the framework of VISM, we consider the following free-energy functional of any phase field $\phi = \phi(\mathbf{x})$ ($\mathbf{x} \in \Omega$):

$$
F_\xi[\phi] = P \int_\Omega \phi^2 \, d\mathbf{x} + \gamma_0 \int_\Omega \left[\frac{\xi}{2} |\nabla \phi|^2 + \frac{1}{\xi} W(\phi) \right] d\mathbf{x}
$$
$$
+ \rho_w \int_\Omega (\phi - 1)^2 U \, d\mathbf{x}
$$
$$
+ \frac{1}{32\pi^2 \varepsilon_0} \left(\frac{1}{\varepsilon_w} - \frac{1}{\varepsilon_m} \right) \int_\Omega (\phi - 1)^2 \left| \sum_{i=1}^N \frac{Q_i(\mathbf{x} - \mathbf{x}_i)}{|\mathbf{x} - \mathbf{x}_i|^3} \right|^2 d\mathbf{x}.
$$
(1)

In the first term of the free-energy functional (1), P is the difference between the pressure inside and outside solute region. For a field ϕ with a low free energy, the integral in the first term of $F_\xi[\phi]$ is the volume of the solute region defined by $\phi \approx 1$. Therefore, the first term describes the volumetric contribution to the immersion of a solute molecule into the solvent.

The second term of the free-energy functional (1) is the effective surface energy of the solute-solvent interface. Here and below, γ_0 is an effective macroscopic surface tension of the solute-solvent interface. It can be different from that for a flat solute-solvent interface. The function $W = W(\phi)$ is a double-well potential. As usual, we choose

$$
W(\phi) = 18\phi^2(1 - \phi)^2,
$$

where the pre-factor 18 is so chosen such that the integral in the γ_0-term in (1) approximates the surface area, as ξ becomes small.

We note that in the sharp-interface VISM free-energy functional, the surface energy is described by the integral on the dielectric boundary Γ of $\gamma_{\text{flat}}(1 - 2\tau H)$, instead of γ_0 alone.[28,29] Here, γ_{flat} is the usual value of surface tension for a macroscopically flat solute-solvent interface. The additional term $-2\gamma_{\text{flat}} \tau H$ is the curvature correction[21,28,29,63–65] where H is the mean curvature (the average of the two principal curvatures) and τ is a fit-parameter often called the Tolman length or coefficient. In practice, one often uses $\tau \approx 1$ Å. For high efficiency, we do not include such a curvature correction to the surface tension in our phase-field formulation. Instead, we us an effective, "global" constant surface tension γ_0. The

value of the effective surface tension γ_0 can be estimated by

$$
\gamma_0 \, \text{area}\,(\Gamma) = \gamma_{\text{flat}} \int_\Gamma (1 - 2\tau H) \, dS.
$$

For a single ion, Γ is a sphere. We can thus use the ionic van der Waals radius and $\tau = 1$ Å to get an estimate for γ_0 from γ_{flat}. In general, γ_0 is still a fit-parameter.

The third term of the free-energy functional (1) describes the solute-solvent interaction that includes both the short-range repulsion due to the excluded volume effect and the long-range attraction. Here, the potential $U = U(\mathbf{x})$ is given by

$$
U(\mathbf{x}) = \sum_{i=1}^N U_{\text{LJ}}^{(i)}(|\mathbf{x} - \mathbf{x}_i|),
$$
(2)

where $U_{\text{LJ}}^{(i)}$ is the Lennard-Jones potential defined by

$$
U_{\text{LJ}}^{(i)}(r) = 4\varepsilon_i \left[\left(\frac{\sigma_i}{r} \right)^{12} - \left(\frac{\sigma_i}{r} \right)^6 \right].
$$
(3)

The parameters ε_i (in units $k_B T$) and σ_i (in units Å) can vary.

The last term in the free-energy functional (1) is the electrostatic part of the solvation free energy. Its sharp-interface version is derived in our previous work[35] based on the Coulomb-field approximation. In this term, ε_0 is the vacuum permittivity, ε_m and ε_w are the relative permittivities of the solute and solvent, respectively, and Q_i is the partial charge of the ith solute atom located at $\mathbf{x}_i$ ($i = 1, \ldots, N$). To reduce the error in approximating the electrostatic energy caused by using a finite region Ω, we replace the region of integral Ω in the last term in (1) by the entire space $\mathbb{R}^3$. Since the region outside Ω is filled with solvent where $\phi = 0$, this is equivalent to adding the quantity

$$
E(\Omega) = \frac{1}{32\pi^2 \varepsilon_0} \left(\frac{1}{\varepsilon_w} - \frac{1}{\varepsilon_m} \right) \int_{\mathbb{R}^3 \setminus \Omega} \left| \sum_{i=1}^N \frac{Q_i(\mathbf{x} - \mathbf{x}_i)}{|\mathbf{x} - \mathbf{x}_i|^3} \right|^2 d\mathbf{x}.
$$
(4)

In our recent work,[53] we have proved mathematically that the family of functionals $F_\xi[\phi]$ parameterized by $\xi > 0$ converges in certain sense (Γ-convergence) to the sharp-interface solvation free-energy functional $F[\Gamma]$ of all solute-solvent interfaces Γ,

$$
F[\Gamma] = P \, \text{vol}\,(\Omega_m) + \gamma_0 \, \text{area}\,(\Gamma) + \rho_w \sum_{i=1}^N \int_{\Omega_w} U_i(|\mathbf{x} - \mathbf{x}_i|) \, d\mathbf{x}
$$
$$
+ \frac{1}{32\pi^2 \varepsilon_0} \left(\frac{1}{\varepsilon_w} - \frac{1}{\varepsilon_m} \right) \int_{\Omega_w} \left| \sum_{i=1}^N \frac{Q_i(\mathbf{x} - \mathbf{x}_i)}{|\mathbf{x} - \mathbf{x}_i|^3} \right|^2 d\mathbf{x},
$$
(5)

where Ω_m and Ω_w are the solute region and solvent region, respectively, that are separated by the sharp, solute-solvent interface Γ. This mathematical result particularly implies the following: if $\phi_\xi = \phi_\xi(\mathbf{x})$ are a sequence of (local) minimizers of the phase-field free-energy functional F_ξ, with the sequence of parameters $\xi \to 0$, then $\phi_\xi(\mathbf{x})$ converges to a characteristic function, $\chi = \chi(\mathbf{x})$, that only takes values 0 and 1 in the entire solvation region Ω. The region Ω_m (m for molecule) defined by $\chi(\mathbf{x}) = 1$ is exactly the solute region containing all

the solute particles $\mathbf{x}_1, \ldots, \mathbf{x}_N$. The region Ω_w (w for water) defined by $\chi(\mathbf{x}) = 0$ is the solvent region. The interface, Γ_min, that separates the solute and solvent regions minimizes the sharp-interface solvation free-energy functional (5). Moreover, $\min F_\xi[\phi]$ (which is the same as $F_\xi[\phi_\xi]$) converges to $\min F[\Gamma]$ (which is the same as $F[\Gamma_\mathrm{min}]$), as ξ approaches 0.

III. COMPUTATIONAL METHODS

To minimize the free-energy functional (1), we solve numerically for a steady-state solution of the partial differential equation of the gradient-flow (i.e., the steepest descent) of the free-energy functional (1): $\partial_t \phi = -\delta_\phi F_\xi[\phi]$, where ∂_t denotes the partial derivative with respect to t and δ_ϕ denotes the variational derivative with respect to ϕ. By routine calculations, we can obtain the variational derivative $\delta_\phi F_\xi[\phi]$. The resulting equation for the phase field $\phi = \phi(\mathbf{x}, t)$ is

$$\partial_t \phi = -2P\,\phi + \gamma_0 \left[\xi \Delta\phi - \frac{1}{\xi} W'(\phi) \right] - 2\rho_\mathrm{w}(\phi - 1)U$$
$$- \frac{1}{16\pi^2 \varepsilon_0} \left(\frac{1}{\varepsilon_\mathrm{w}} - \frac{1}{\varepsilon_\mathrm{m}} \right)(\phi - 1) \left| \sum_{i=1}^{N} \frac{Q_i(\mathbf{x} - \mathbf{x}_i)}{|\mathbf{x} - \mathbf{x}_i|^3} \right|^2 . \quad (6)$$

We solve this equation together with some initial condition $\phi(\mathbf{x}, 0) = \phi_0(\mathbf{x})$ for some given $\phi_0(\mathbf{x})$ and the periodical boundary condition.

We use several kinds of initial phase fields $\phi_0(\mathbf{x})$ in the initial condition for solving the evolution equation (6). The first one corresponds to a tight wrap: a surface that is close to the van der Waals surface of the solute atoms. The second one is a loose wrap: a surface that loosely encloses all the solute atoms. An example of such a loose wrap is a sphere of large radius. The third one is a combination of tight and loose wraps.

We choose our computational domain to be $\Omega = (-L, L)^3$ with a given $L > 0$ and cover it by a uniform grid of N_s^3 grid points for some integer $N_s > 1$. We label all the three-dimensional grid points by (i, j, k) with $i, j, k = 0, 1, \ldots, N_s$. We also choose a time step $\Delta t > 0$ and set $t_n = n\Delta t$ ($n = 0, 1, \ldots$). For a given function $u = u(\mathbf{x}, t)$, we denote by $u^{(n)}(\mathbf{x})$ an approximation of $u(\mathbf{x}, t_n)$ at time t_n and by $u_{i,j,k}^n$ an approximation of $u(\mathbf{x}_{i,j,k}, t_n)$ at the grid point $\mathbf{x}_{i,j,k}$ and time t_n. We use a semi-implicit scheme for the time discretization of Eq. (6). We treat implicitly the terms $-2P\phi$ and $\gamma_0 \xi \Delta\phi$ in the right-hand side of (6), and treat the other terms explicitly. As a result, we obtain the time discretization:

$$\gamma_0 \xi \Delta t \Delta \phi^{(n+1)} - (1 + 2P\Delta t)\phi^{(n+1)}$$
$$= \frac{\gamma_0 \Delta t}{\xi} W'\left(\phi^{(n)}\right) - \phi^{(n)}$$
$$+ \Delta t \left(\phi^{(n)} - 1\right) \left[2\rho_\mathrm{w} U + \frac{1}{16\pi^2 \varepsilon_0} \left(\frac{1}{\varepsilon_\mathrm{w}} - \frac{1}{\varepsilon_\mathrm{m}} \right) \right.$$
$$\left. \times \left| \sum_{i=1}^{N} \frac{Q_i(\mathbf{x} - \mathbf{x}_i)}{|\mathbf{x} - \mathbf{x}_i|^3} \right|^2 \right], \quad n = 0, 1, \ldots.$$

For each $n \geq 0$, we use the Fourier spectral method to solve the above elliptic equation with periodic boundary condition to obtain $\phi^{(n+1)}$. If the difference $F[\phi^{(n+1)}] - F[\phi^{(n)}]$ between the free-energy values of two consecutive iterates $\phi^{(n)}$ and $\phi^{(n+1)}$ is smaller than a tolerance (e.g., 10^{-6}), then we stop the computation and use $\phi^{(n+1)}$ as the steady-state solution.

To evaluate the electrostatic energy, we need to compute $E(\Omega)$ defined in (4). We notice that each $\mathbf{x}_i$ is inside Ω. Moreover, $(\mathbf{x} - \mathbf{x}_i)/|\mathbf{x} - \mathbf{x}_i|^3 = -\nabla(1/|\mathbf{x} - \mathbf{x}_i|)$ and $\Delta(1/|\mathbf{x} - \mathbf{x}_i|) = 0$ in $\mathbb{R}^3 \setminus \Omega$. Therefore, we have by Green's identity that for any i and j with $1 \leq i, j \leq N$,

$$\int_{\mathbb{R}^3 \setminus \Omega} \frac{(\mathbf{x} - \mathbf{x}_i) \cdot (\mathbf{x} - \mathbf{x}_j)}{|\mathbf{x} - \mathbf{x}_i|^3 |\mathbf{x} - \mathbf{x}_j|^3} d\mathbf{x}$$
$$= \int_{\mathbb{R}^3 \setminus \Omega} \nabla\left(\frac{1}{|\mathbf{x} - \mathbf{x}_i|} \right) \cdot \nabla\left(\frac{1}{|\mathbf{x} - \mathbf{x}_j|} \right) d\mathbf{x}$$
$$= -\int_{\partial\Omega} \frac{1}{|\mathbf{x} - \mathbf{x}_i|} \frac{\partial}{\partial n}\left(\frac{1}{|\mathbf{x} - \mathbf{x}_j|} \right) dS_\mathbf{x}$$
$$= \int_{\partial\Omega} \frac{\mathbf{n}(\mathbf{x}) \cdot (\mathbf{x} - \mathbf{x}_j)}{|\mathbf{x} - \mathbf{x}_i| \, |\mathbf{x} - \mathbf{x}_j|^3} dS_\mathbf{x},$$

where $\partial/\partial n$ denotes the normal derivative along the boundary $\partial\Omega$ of Ω, and $\mathbf{n}(\mathbf{x})$ is the unit normal to $\partial\Omega$ at $\mathbf{x}$ pointing from inside to outside of Ω. If $i \neq j$ then we have a symmetric form:

$$2\int_{\mathbb{R}^3 \setminus \Omega} \frac{(\mathbf{x} - \mathbf{x}_i) \cdot (\mathbf{x} - \mathbf{x}_j)}{|\mathbf{x} - \mathbf{x}_i|^3 |\mathbf{x} - \mathbf{x}_j|^3} d\mathbf{x}$$
$$= \int_{\partial\Omega} \frac{\mathbf{n}(\mathbf{x})}{|\mathbf{x} - \mathbf{x}_i| \, |\mathbf{x} - \mathbf{x}_j|} \cdot \left(\frac{\mathbf{x} - \mathbf{x}_i}{|\mathbf{x} - \mathbf{x}_i|^2} + \frac{\mathbf{x} - \mathbf{x}_j}{|\mathbf{x} - \mathbf{x}_j|^2} \right) dS_\mathbf{x}.$$

Consequently,

$$E(\Omega) = \frac{1}{32\pi^2 \varepsilon_0} \left(\frac{1}{\varepsilon_\mathrm{w}} - \frac{1}{\varepsilon_\mathrm{m}} \right) \left[\sum_{i=1}^{N} Q_i^2 \int_{\partial\Omega} \frac{\mathbf{n}(\mathbf{x}) \cdot (\mathbf{x} - \mathbf{x}_i)}{|\mathbf{x} - \mathbf{x}_i|^4} dS_\mathbf{x} \right.$$
$$+ \sum_{1 \leq i < j \leq N} Q_i Q_j \int_{\partial\Omega} \frac{\mathbf{n}(\mathbf{x})}{|\mathbf{x} - \mathbf{x}_i| \, |\mathbf{x} - \mathbf{x}_j|}$$
$$\left. \cdot \left(\frac{\mathbf{x} - \mathbf{x}_i}{|\mathbf{x} - \mathbf{x}_i|^2} + \frac{\mathbf{x} - \mathbf{x}_j}{|\mathbf{x} - \mathbf{x}_j|^2} \right) dS_\mathbf{x} \right].$$

We now test our theory and method on a one-particle system ($N = 1$). We place a single point charge Q at the origin immersed in water. As the one-particle system is radially symmetric, the phase-field free-energy functional (1) reduces to that of radially symmetric phase fields $\phi = \phi(r)$ ($N = 1$ and $Q_1 = Q$):

$$F[\phi] = 4\pi P \int_0^\infty [\phi(r)]^2 r^2 \, dr$$
$$+ 4\pi \gamma_0 \int_0^\infty \left[\frac{\xi}{2} |\phi'(r)|^2 + \frac{1}{\xi} W(\phi(r)) \right] r^2 \, dr$$
$$+ 4\pi \rho_\mathrm{w} \int_0^\infty [\phi(r) - 1]^2 \, U(r) r^2 \, dr$$
$$+ \frac{Q^2}{8\pi \varepsilon_0} \left(\frac{1}{\varepsilon_\mathrm{w}} - \frac{1}{\varepsilon_\mathrm{m}} \right) \int_0^\infty \frac{1}{r^2} [\phi(r) - 1]^2 \, dr, \quad (7)$$

TABLE I. A comparison of numerical results obtained by the phase-field calculations (solving the Euler-Lagrange equation (8)) and by the sharp-interface calculations (minimizing numerically the function $G[R]$ in (9)) for the solvation of a single-particle system. The sharp-interface results are presented in the last column. See the text for the units.

Q	Optimal radii/energy	$\xi = 0.5$	$\xi = 0.2$	$\xi = 0.05$	$\xi = 0.02$	Sharp-interface
0.0	$R_{\min}$	3.003	3.026	3.045	3.048	3.054
	F_{surf}	19.861	20.153	20.389	20.426	20.511
	F_{vdW}	-2.595	-2.635	-2.610	-2.583	-2.644
	F_{elec}	0.000	0.000	0.000	0.000	0.000
	F_{tot}	17.267	17.518	17.779	17.8431	17.867
0.5	$R_{\min}$	2.910	2.933	2.953	2.954	2.960
	F_{surf}	18.696	18.937	19.177	19.195	19.267
	F_{vdW}	-1.056	-1.060	-1.053	-0.986	-1.054
	F_{elec}	-23.032	-23.157	-23.171	-23.193	-23.173
	F_{tot}	-5.391	-5.280	-5.0470	-4.984	-4.960
1.0	$R_{\min}$	2.724	2.756	2.764	2.768	2.771
	F_{surf}	17.024	16.842	16.863	16.856	16.886
	F_{vdW}	5.116	5.138	5.118	5.223	5.113
	F_{elec}	-99.529	-99.256	-99.131	-99.106	-99.012
	F_{tot}	-77.389	-77.276	-77.150	-77.027	-77.017
1.5	$R_{\min}$	2.547	2.566	2.585	2.589	2.593
	F_{surf}	18.510	16.201	15.132	14.921	14.782
	F_{vdW}	19.127	18.532	18.143	18.056	17.971
	F_{elec}	-245.685	-241.735	-239.117	-238.521	-238.105
	F_{tot}	-208.048	-207.002	-205.842	-205.544	-205.354
2.0	$R_{\min}$	2.403	2.422	2.440	2.445	2.448
	F_{surf}	28.520	19.597	14.854	13.855	13.178
	F_{vdW}	45.171	41.678	39.565	39.123	38.757
	F_{elec}	-483.156	-464.071	-452.592	-450.081	-448.317
	F_{tot}	-409.465	-402.796	-398.173	-397.103	-396.381

where $U(r)$ is given by (3) with $N = 1$, $\varepsilon_1 = \varepsilon$, and $\sigma_1 = \sigma$. Instead of solving the corresponding time-dependent, gradient-flow equation (6), we minimize the functional by solving the corresponding Euler-Lagrange equation:

$$2Pr^2\phi - \gamma_0\xi(r^2\phi')' + \frac{\gamma_0}{\xi}r^2 W'(\phi)$$
$$+ \left[2\rho_{\text{w}}r^2 U(r) + \frac{Q^2}{16\pi^2\varepsilon_0}\left(\frac{1}{\varepsilon_{\text{w}}} - \frac{1}{\varepsilon_{\text{m}}}\right)\frac{1}{r^2}\right](\phi - 1) = 0. \tag{8}$$

We use the adaptive solver BVP4C in MATLAB to solve this ordinary differential equation together with some boundary conditions in the range $0 \leq r \leq R_\infty$ with $R_\infty = 25$ Å.

We compare our results of phase-field computations for the one-particle system with those of the sharp-interface implementation. For a one-particle system, the sharp-interface free-energy functional (5) is a one-variable function of the radius R of the solute sphere centered at the origin. It is given by Ref. 35:

$$G[R] = \frac{4}{3}\pi P R^3 + 4\pi\gamma_0 R^2 + 16\pi\rho_{\text{w}}\varepsilon\left(\frac{\sigma^{12}}{9R^9} - \frac{\sigma^6}{3R^3}\right)$$
$$+ \frac{Q^2}{8\pi\varepsilon_0 R}\left(\frac{1}{\varepsilon_{\text{w}}} - \frac{1}{\varepsilon_{\text{m}}}\right). \tag{9}$$

This one-variable function can be minimized numerically with a very high accuracy.

We use the following parameters: $P = 0$, $T = 300$ K, $\gamma_0 = 0.175$ $k_{\text{B}}T/\text{Å}^2$ with k_{B} the Boltzmann constant, $\rho_{\text{w}} = 0.0333$ Å^{-3}, $\varepsilon = 0.3\,k_{\text{B}}T$, $\sigma = 3.5$ Å, $\varepsilon_0 = 1.4321 \times 10^{-4}\,\text{e}^2/(k_{\text{B}}T\,\text{Å})$, $\varepsilon_{\text{m}} = 1$, and $\varepsilon_{\text{w}} = 80$. We test on a set of Q-values (in units e): $Q = 0.0, 0.5, 1.0, 1.5, 2.0$. We use both the sharp-interface and phase-field models to calculate the optimal radius $R_{\min}$, the total minimum free energy F_{tot}, and the corresponding surface energy F_{surf}, solute-solvent van der Waals interaction energy F_{vdW}, and the electrostatic energy F_{elec}, respectively. For our phase-field calculations, we use different values of the numerical parameter ξ (in units Å). Table I shows our computational results. It is clear that as ξ becomes smaller, the result of the phase-field model is also closer to that of the sharp-interface model.

IV. APPLICATIONS

We now apply our phase-field variational implicit-solvent model (P-VISM) to a few single ions, a two-plate system, and the two-domain protein BphC. For each of these systems, we use the following parameters: $\xi = 0.5$ Å, $P = 0$ bar, $T = 300$ K, $\rho_{\text{w}} = 0.0333\,\text{Å}^{-3}$, $\varepsilon_0 = 1.4321 \times 10^{-4}\,\text{e}^2/(k_{\text{B}}T\,\text{Å})$, $\varepsilon_{\text{m}} = 1$, and $\varepsilon_{\text{w}} = 80$. All the effective surface tension γ_0, the Lennard-Jones parameters ε_i and σ_i ($1 \leq i \leq N$), and the partial charges Q_i ($1 \leq i \leq N$) will be specified later. In all of our computations, we set the computational box to be $\Omega = (-L, L)^3$ with $L = 20$ Å and use a grid with 256×256

TABLE II. Solvation free energies ($k_B T$) obtained by P-VISM, VISM, and experiment[66] for single ions K^+, Na^+, Cl^-, and F^-. The Lennard-Jones parameters ε ($k_B T$) and σ (Å) are taken from Ref. 67. Different effective values of the surface tension γ_0 ($k_B T/Å^2$) are used in the P-VISM calculations reported in the fourth and fifth columns, respectively. The percentages in these two columns are the relative errors compared with the experiment.

Ions	ε	σ	P-VISM ($\gamma_0 = 0.175$)	P-VISM ($\gamma_0 = 0.0583$)	VISM	Experiment
K^+	0.008	3.85	-103.7 (11.7%)	-112.0 (4.6%)	-112.3	-117.5
Na^+	0.008	3.49	-124.4 (14.4%)	-132.9 (8.6%)	-131.1	-145.4
Cl^-	0.21	3.78	-114.3 (15.5%)	-125.9 (7.0%)	-126.7	-135.4
F^-	0.219	3.3	-162.1 (12.4%)	-170.2 (8.1%)	-171.9	-185.2

$\times$ 256 grid points to cover Ω. We also set the time step $\Delta t = 0.1$. After the final steady-state solution ϕ is reached, we compute the 1/2-level set of ϕ, i.e., $\{\mathbf{x} \in \Omega : \phi(\mathbf{x}) = 1/2\}$, as the sharp solute-solvent interface. In calculating the electrostatic part of the solvation energy for single anions, we use a new phase field rescaled from our P-VISM equilibrium phase field, effectively shrinking the dielectric boundary.[35]

A. Single ions

We use our P-VISM to calculate the solvation free energy for each of the single ions K^+, Na^+, Cl^-, and F^-. As in the sharp-interface VISM,[35] we calculate the electrostatic part of the solvation free energy for anions Cl^- and F^- using a shifted dielectric boundary that is obtained by shrinking the optimal solute-solvent boundary obtained by our P-VISM by 1 Å, which is the length of the water OH bond, to include the asymmetry effect.[29,35,36] Specifically, we first compute a free-energy minimizing phase field ϕ. We then calculate its 1/2-level set which is approximately a sphere, and also calculate the radius r_0 of this sphere. We further define a new phase field $\phi^*(\mathbf{x}) = \phi(r_0 \mathbf{x}/(r_0 - 1))$ and use it for calculating the electrostatic part of the free energy. Note that the 1/2-level set of ϕ^* is a sphere approximately of radius $r_0 - 1$, which is the shifted dielectric boundary.

In Table II, we display the solvation free energies for each of the four ions by our P-VISM, the sharp-interface VISM (marked VISM),[35] and experiment[66] (converted from kJ/mol to $k_B T$). In the sharp-interface VISM calculations, the Tolman coefficient is $\tau = 1$ Å. We see that a good agreement among our P-VISM, VISM, and experiment is reached. In particular, a smaller value of the effective surface tension provides a better estimate of the solvation free energy.

B. Two parallel plates

We now consider the system of two parallel molecular plates that has been studied by the molecular dynamics simulations[68] and by the sharp-interface VISM.[35] Each plate consists of 6×6 fixed CH_2 atoms with the atom-to-atom distance $d_0 = 2.1945$ Å. The plate has a square length of about 30 Å. The two plates are placed in parallel with a center-to-center distance d. We use the usual value of the surface tension $\gamma_0 = 0.175\, k_B T/Å^2$. The Lennard-Jones parameters for the solute-solvent van der Waals interaction are $\varepsilon = 0.3\, k_B T$ and $\sigma = 3.5$ Å, same for all the solute atoms. To study the

charge effect, as in Ref. 35, we assign central charges q_1 and q_2 to the first and second plates, respectively, with $|q_1| = |q_2|$. The total charges of these two plates are $36q_1$ and $36q_2$, respectively. We choose the values of (q_1, q_2) to be $(0\,\mathrm{e}, 0\,\mathrm{e})$, $(+0.1\,\mathrm{e}, -0.1\,\mathrm{e})$, $(+0.1\,\mathrm{e}, +0.1\,\mathrm{e})$, $(+0.2\,\mathrm{e}, -0.2\,\mathrm{e})$, and $(+0.2\,\mathrm{e}, +0.2\,\mathrm{e})$. For each of some selected values of d, we solve Eq. (6) to obtain the steady-state solution which in turn determines a stable equilibrium solute-solvent interface. We use two different types of initial phase fields. One is a tight wrap, which consists of two surfaces, tightly wrapping up the two plates, respectively. The other corresponds to a large box containing both of the plates.

Figure 1 shows typical snapshots from our numerical relaxation. We observe that, with the plate-plate separation $d = 16$ Å and partial charges $(q_1, q_2) = (0.1\,\mathrm{e}, 0.1\,\mathrm{e})$, there are two stable, equilibrium conformations. One is a wet state in which the solute-solvent interface wraps tightly around the solute atoms, and the solvent molecules get in between the two plates. This state is reached with a tight initial; cf. the last one in the top row. The other is a (partially) dry state in which the solvent molecules are repelled. This state is reached with a loose initial; cf. the last one in the bottom row.

To study the charge effect to the wetting and drying of the plates, we fix the plates with the plate-plate separation $d = 12$ Å and assign partial charges $(q_1, q_2) = (0\,\mathrm{e}, 0\,\mathrm{e})$, $(0.2\,\mathrm{e}, 0.2\,\mathrm{e})$, and $(-0.2\,\mathrm{e}, 0.2\,\mathrm{e})$, respectively. For each pair of partial charges, we numerically relax our P-VISM functional using a loose initial. In Figure 2, we show the three final, stable, equilibrium conformations of the two plates. We see that if the plates are equally like-charged, then a stable capillary bubble remains but with a tighter surface when compared to the uncharged case $q_1 = q_2 = 0\,\mathrm{e}$. This is because the oppositely directed electrostatic field cancels out in the void and the water distribution is hardly affected. If the plates are charged oppositely, capillary evaporation is suppressed and the final state is wet. This is because the strong electric field between the plates drags the polar water into the void. Overall, the charging suppresses the capillary evaporation, showing the sensitive coupling between electrostatics and hydrophobicity in aqueous solvation. We note that the P-VISM equilibrium surfaces obtained with tight initials are all very similar to the right one in Figure 2, regardless how charges are distributed.

We now study the potential of mean forces (PMF) with the reaction coordinate being the plate-plate separation d (in Å). Let ϕ_d be a free-energy minimizing phase field corresponding to a given reaction coordinate d. The total
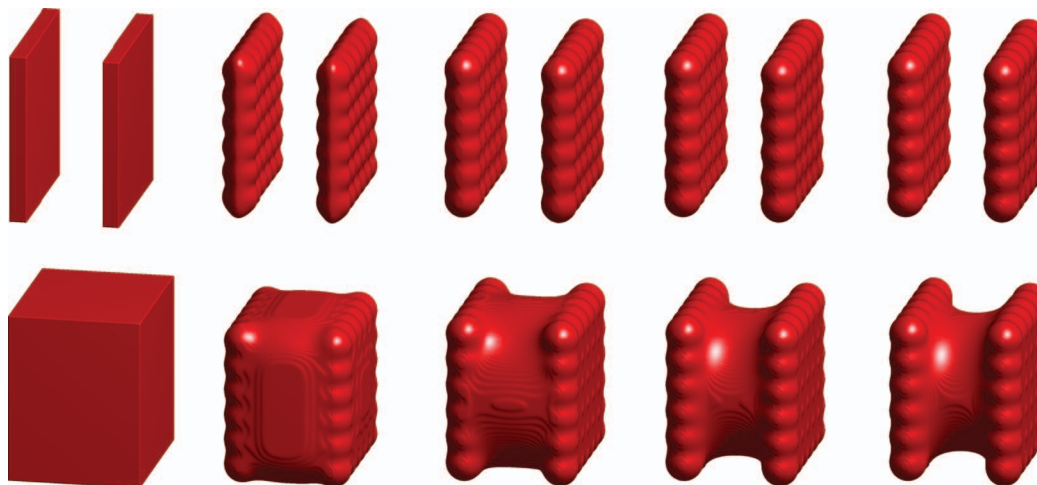
FIG. 1. Snapshots from numerical relaxation of the two-plate system. A red region indicates the solute region without solvent. Outside the red region is the solvent region. Each red surface is defined as the 1/2-level set of a phase-field function $\{\mathbf{x} : \phi(\mathbf{x}, t) = 1/2\}$ at some relaxation time t, where $\phi(\mathbf{x}, t)$ solves Eq. (6). In these computations, the plate-plate separation is fixed to be $d = 16$ Å and the partial charges are fixed to be $(q_1, q_2) = (0.1\,\text{e}, 0.1\,\text{e})$. In each row from left to right, the first is the initial surface and the last is the corresponding final, steady-state surface.

solvation free energy $F[\phi_d]$ is the sum of the geometrical part (the surface energy) $F_{\text{geom}}[\phi_d]$, the solute-solvent van der Waals interaction energy $F_{\text{vdW}}[\phi_d]$, and the electrostatic energy $F_{\text{elec}}[\phi_d]$:

$$F[\phi_d] = F_{\text{geom}}[\phi_d] + F_{\text{vdW}}[\phi_d] + F_{\text{elec}}[\phi_d].$$

As in Refs. 35 and 36, we define the (total) PMF by

$$G_{\text{tot}}^{\text{PMF}}(d) = G_{\text{geom}}^{\text{PMF}}(d) + G_{\text{vdW}}^{\text{PMF}}(d) + G_{\text{elec}}^{\text{PMF}}(d),$$

with

$$G_{\text{geom}}^{\text{PMF}}(d) = F_{\text{geom}}[\phi_d] - F_{\text{geom}}[\phi_\infty],$$

$$G_{\text{vdW}}^{\text{PMF}}(d) = F_{\text{vdW}}[\phi_d] - F_{\text{vdW}}[\phi_\infty]$$
$$+ \sum_{i \in \text{Plate I}} \sum_{j \in \text{Plate II}} U_{i,j}(|\mathbf{x}_i - \mathbf{x}_j|),$$

$$G_{\text{elec}}^{\text{pmf}}(d) = F_{\text{elec}}[\phi_d] - F_{\text{elec}}[\phi_\infty]$$
$$+ \frac{1}{4\pi\varepsilon_{\text{m}}\varepsilon_0} \sum_{i \in \text{Plate I}} \sum_{j \in \text{Plate II}} \frac{Q_i Q_j}{|\mathbf{x}_i - \mathbf{x}_j|}.$$
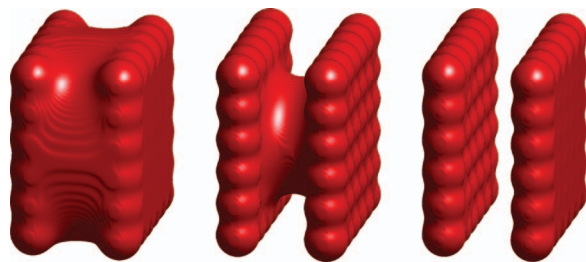

FIG. 2. Stable equilibrium solute-solvent surfaces of the two-plate system obtained by the P-VISM calculations with loose initials. A red region indicates the solute region without solvent. Outside the red region is the solvent region. Each red surface is defined as the 1/2-level set of a phase-field function $\{\mathbf{x} : \phi(\mathbf{x}, t) = 1/2\}$ at some relaxation time t, where $\phi(\mathbf{x}, t)$ solves Eq. (6). The plate-plate separation is fixed to be $d = 12$ Å. From left to right, the partial charges are $(q_1, q_2) = (0\,\text{e}, 0\,\text{e})$, $(0.2\,\text{e}, 0.2\,\text{e})$, and $(-0.2\,\text{e}, 0.2\,\text{e})$, respectively.

Here a quantity at ∞ is understood as the limit of that quantity at a coordinate d' as $d' \to \infty$, and $U_{i,j}$ is the Lennard-Jones interaction potential between $\mathbf{x}_i$ and $\mathbf{x}_j$. A quantity at ∞ can be calculated by doubling that of a single plate.

For a given reaction coordinate d there can be multiple stable equilibrium phase fields ϕ_d that are local minimizers of the P-VISM free-energy functional. Different local minimizers for the same coordinate d define multiple local minimum free energies. Therefore, the PMF can have multiple branches along the reaction coordinate d, and hence can lead to hysteresis. Strictly speaking, therefore, our PMFs are different from those defined using a Boltzmann average over all possible minimizers. Rather, our PMFs reflect possible branches of the VISM free energy along the reaction coordinate d.

Figure 3 shows the two different PMF branches for the two-plate system with several, different values of partial charges. These PMFs exhibit clearly the bimodal behavior and hysteresis of the system. For the neutral plates (cf. Figure 3, left), a strong hysteresis is present for $6 \lesssim d \lesssim 16$ Å. Adding charges influences the free-energy branches and hysteresis as shown in Figure 3 (middle and right). However, only in the case of oppositely charged plates, the changes are significant as a strong electrostatic field develops in between the hydrophobic plates.

In Figures 4 and 5, we plot the different components of the PMF with loose and tight initial surfaces, respectively. For the loose initials (Figure 4), the geometric part displays a strong attraction below a critical distance d_c at which capillary evaporation begins. The crossover distance decreases from $d_c \simeq 20$ Å for $(q_1, q_2) = (-0.2\,\text{e}, +0.2\,\text{e})$ down to 9 Å for $(q_1, q_2) = (0\,\text{e}, 0\,\text{e})$. The value 20 Å is larger than 14 Å predicted by the sharp-interface VISM where the curvature correction was included. Note that the opposite charging has a much stronger effect than like-charging due to the electrostatic field distribution discussed above. Also the solute-solvent vdWS part of the interaction is strongly affected by electrostatics due to the very different surface geometries induced by charging.
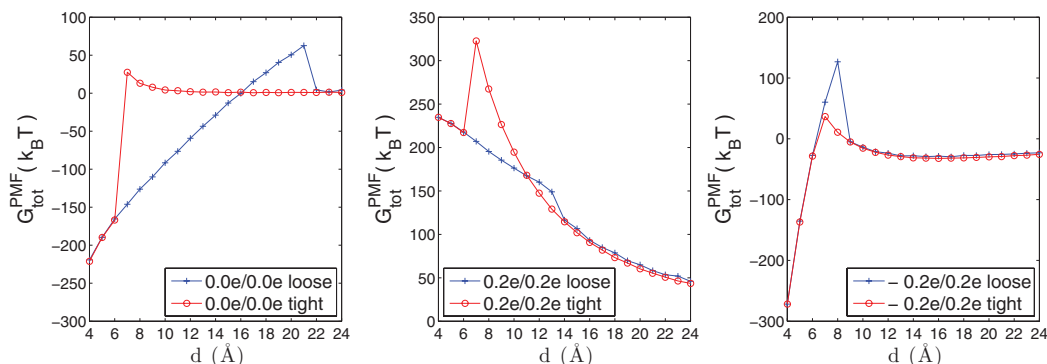
FIG. 3. The two PMF branches corresponding to the wet (red and circles) and dry (blue and +) states, in certain range of d, for the two plates carrying different partial charges (q_1, q_2).

Both curves $G_{\text{geom}}^{\text{PMF}}(d)$ and $G_{\text{vdW}}^{\text{PMF}}(d)$ demonstrate the strong sensitivity of nonpolar hydration to local electrostatics when capillary evaporation occurs and very "soft" surfaces are present. For the surfaces resulting from the tight initials (Figure 5), the situation is a bit less sensitive to electrostatics as the final surface is closer to the vdWS surface for $d_c \gtrsim 6$ Å.

C. The protein BphC

We now apply our P-VISM to BphC, a key enzyme of biphenyl biodegradation pathway in *Pseudomonos sp*. The functional unit of this protein is a homo-octamer, and each subunit consists of two domains. This system has been carefully studied by molecular dynamics simulations[26] and by the sharp-interface VISM.[35,36] These studies indicate a strong interplay between hydrophobic and electrostatic contributions to the structure of protein-water interface. Our study here is

close to that by the sharp-interface VISM.[35,36] We choose several values of the domain separation d for which $d = 0$ is the native configuration in crystal structure (PDB code: 1dhy). For each fixed d value, we apply our P-VISM to compute the solvation free energy and the equilibrium BphC surface.

In Figure 6 we show our P-VISM computational results of six BphC surfaces at three different domain separations with and without atomic partial charges. In these calculations, we set the effective surface tension to be $\gamma_0 = 0.13\,k_{\text{B}}T/\text{Å}^2$. At $d = 8$ Å, the P-VISM identifies the inter domain region as partially solvent excluded when atomic charges are included, and as completely solvent excluded without any atomic partial charges. The interface wraps around the protein more tightly with charges than that without them due to the attractive nature of the polar interactions between solute and solvent. At $d = 14$ Å, the uncharged and charged BphC molecules pose topologically distinct solute-solvent interfaces. With polar
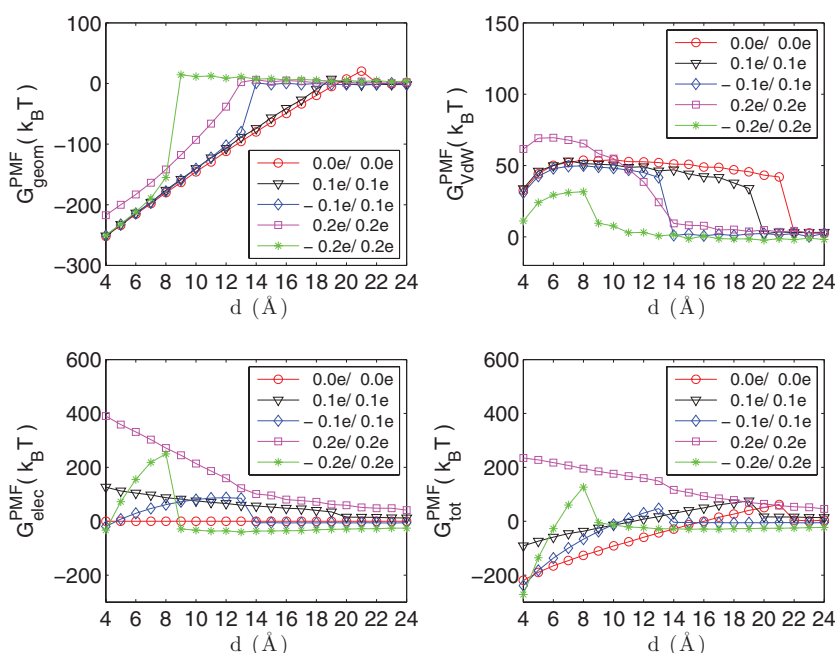

FIG. 4. Different components of the PMF for the two-plate system for different charge combinations (q_1, q_2) (see legend) obtained by the phase-field VISM with loose initial surfaces.
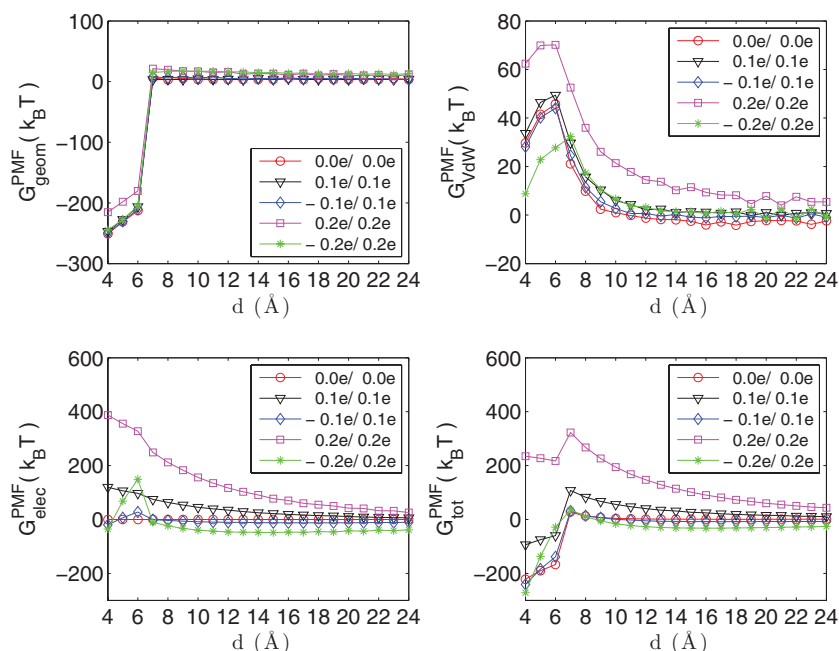
FIG. 5. Different components of the PMF for the two-plate system for different charge combinations (q_1, q_2) (see legend) obtained by the phase-field VISM with tight initial surfaces.

interactions, both domains are completely solvated. By contrast, the center of the domain interface still remains low water occupancy without electrostatic interactions. At $d = 16$ Å, such topological distinction is more significant. All these are consistent with the results from atomistic simulations, where dewetting extends to a much greater region without polar interactions. It is clear that charges modify the solute-solvent interface dramatically for BphC. Compared with traditional surfaces, such as vdWS, SES, or SAS, the P-VISM surfaces are topologically similar at small and large inter domain separations. However, a traditional surface would break into two independent surfaces for large d regardless charge distribution.

To test how the effective surface tension can qualitatively change the equilibrium structures of the protein BphC, we perform our P-VISM computations with three different values of the effective surface tension $\gamma_0 = 0.175, 0.13, 0.08\,k_B T/\text{Å}^2$, respectively. We fix the protein-protein separation $d = 14$ Å and use loose initials. The computational results are shown in Figure 7. Without charges, the change of the effective surface tension can affect significantly the equilibrium conformations. However, such variation of effective surface tension does not affect the equilibrium conformations when charges are turned on. This indicates that the electrostatics dominates the hydrophobic interaction in the system.
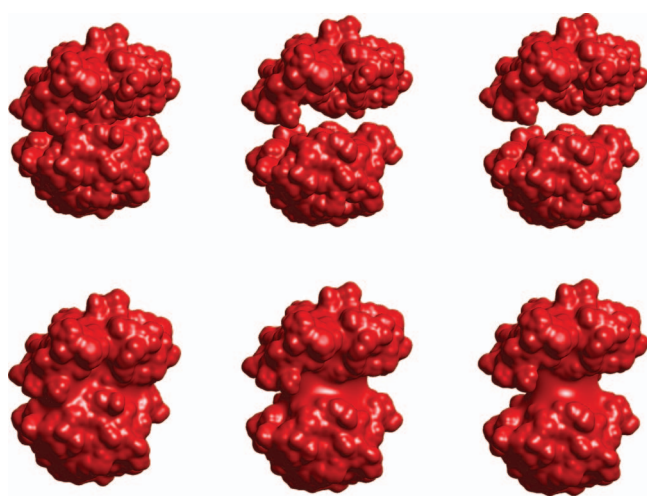

FIG. 6. The phase-field VISM calculations of the BphC with loose initials. Red indicates a solute region. Upper row: with partial charges. Lower row: without partial charges. From the left to right in each row, the protein-protein separation is $d = 8, 14, 16$ Å, respectively.
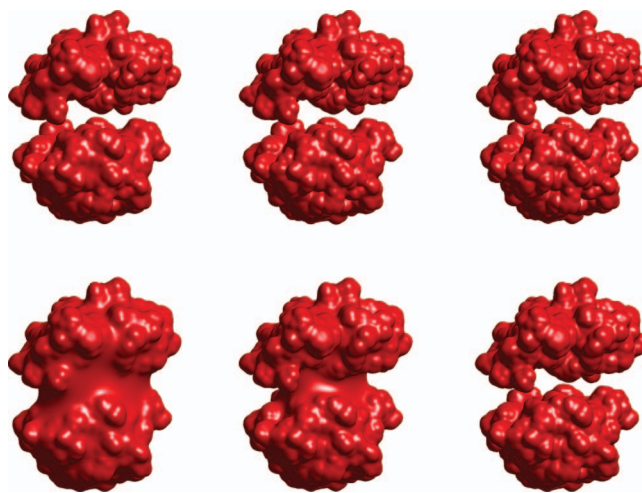

FIG. 7. P-VISM surfaces of BphC with loose initials and $d = 14$ Å. Red indicates a solute region. Upper row: with partial charges. Lower row: without partial charges. From left column to right column: $\gamma_0 = 0.175, 0.13, 0.08\,k_B T/\text{Å}^2$.

V. CONCLUSIONS

We have developed a new P-VISM for the prediction of equilibrium structures and solvation free energies of charged molecules in an aqueous solution. This model is based on the minimization of a solvation free-energy functional of all phase fields. A phase field $\phi = \phi(\mathbf{x})$ with a low solvation free energy partitions the entire solvation region into the solute region where $\phi(\mathbf{x}) \approx 1$, the solvent region where $\phi(\mathbf{x}) \approx 0$, and a thin transition layer that defines a diffuse solute-solvent interface. As in the sharp-interface variational implicit-solvent approach, the free-energy functional consists of surface energy, solute-solvent van der Waals interaction energy of short-range repulsion and long-range attraction, and the electrostatic energy. The surface energy is modeled by the integral of the gradient of phase field and a double-well potential of phase field, with a proper numerical scaling. The electrostatic interaction is described by the Coulomb-field approximation. In our recent work,[53] we have proved mathematically that our phase-field free-energy functional converges in certain sense to the sharp-interface one as the numerical parameter approaches zero. We minimize the free-energy functional by solving the time-dependent, gradient-flow equation with an initial phase field often chosen as a tight or loose surface enclosing all the solute particles. We design and implement numerical methods to solve such an equation for steady state solutions.

Our applications to a few single ions, two parallel charged plates, and the protein BphC have shown that our theory and methods can predict qualitatively well the solvation free energies for these systems. Moreover, we have been able to capture multiple equilibrium states of wet and dry for the two-plate system and the protein BphC. Such multiple states exist generally in other biomolecules in solution. They lead to the system hysteresis and fluctuations. But they are hard to be described by implicit-solvent models of fixed-surface type. Further, we have found from two plates to a complex protein that charges impact strongly on the process of hydration and dehydration. These results are in parallel to those obtained by our previous studies using a sharp-interface VISM.[35,36] In addition, we have found that by using an effective surface tension, we can provide relatively good estimates of the solvation free energies. The variation of effective surface tension can change the conformation of a nonpolar molecule. Such variation, however, affects little to a charged molecule.

We now compare our P-VISM with the previously developed sharp-interface VISM. First, in a real molecular system, a solute-solvent interface fluctuates,[69] and hence is really a diffuse interface. A phase-field description of such an interface seems to be more reasonable. However, such a description introduces a fit-parameter, the numerical parameter ξ, that needs to be adjusted. Second, in our current P-VISM, we do not have the curvature correction in the surface energy. Such correction can be included in the sharp-interface VISM. Sometimes, this curvature correction is crucial in providing an accurate estimate of the solvation free energy. As we have found, such curvature correction can be achieved by using an effective surface tension. Moreover, the variation of such surface tension does not strongly affect a charged molecular sys-

tem. Third, both the sharp-interface VISM implemented by the level-set method and our current P-VISM are similar in terms of accuracy and efficiency. For the phase-field implementation, one cannot choose the numerical parameter ξ to be too small, as otherwise one will need to have many more grid points to resolve the interface. This will then lead to the computational system to be too large, if one does not use local adaptivity which itself may slow down the computation. Finally, the most important reason that we develop our current P-VISM is that fluctuations of solute-solvent interfaces, critically important in biomolecular conformational changes, are in general hard to describe through a sharp-interface description.

As in many phase-field applications, we have treated the parameter ξ as a purely numerical parameter. (In the literature of phase filed, ε is often used to denote this numerical parameter.) In general, this parameter ξ describes the interfacial thickness. In the context of molecular solvation, such thickness of a solute-solvent interface can be curvature dependent. It is determined by molecular roughness and the interfacial fluctuations.[69–71] In this work, we select this parameter ξ to be a fraction of 1 Å for the molecular roughness. It is interesting to further study how the interfacial fluctuations can change such a thickness and how such changes can be incorporated in our phase-field model.

We are currently working to incorporate the Poisson-Boltzmann equation into our P-VISM to better describe the electrostatic interaction. We are also developing a method to include system fluctuations through a phase-field description. In future it is possible to combine our P-VISM with molecular dynamics simulations to describe hydration shells, the distribution of water molecules, and other more detailed molecular properties of a solvation system.

[1]J. Tomasi and M. Persico, Chem. Rev. **94**, 2027 (1994).
[2]C. J. Cramer and D. G. Truhlar, Chem. Rev. **99**, 2161 (1999).
[3]B. Roux and T. Simonson, Biophys. Chem. **78**, 1 (1999).
[4]M. Feig and C. L. Brooks III, Curr. Opin. Struct. Biol. **14**, 217 (2004).
[5]B. Lee and F. M. Richards, J. Mol. Biol. **55**, 379 (1971).
[6]F. M. Richards, Annu. Rev. Biophys. Bioeng. **6**, 151 (1977).
[7]M. L. Connolly, J. Appl. Crystallogr. **16**, 548 (1983).
[8]T. J. Richmond, J. Mol. Biol. **178**, 63 (1984).
[9]M. L. Connolly, J. Mol. Graphics **11**, 139 (1993).
[10]M. E. Davis and J. A. McCammon, Chem. Rev. **90**, 509 (1990).
[11]F. Fixman, J. Chem. Phys. **70**, 4995 (1979).
[12]P. Grochowski and J. Trylska, Biopolymers **89**, 93 (2008).
[13]B. Li, SIAM J. Math. Anal. **40**, 2536 (2009).

[14]K. A. Sharp and B. Honig, J. Phys. Chem. **94**, 7684 (1990).

[15]D. Bashford and D. A. Case, Annu. Rev. Phys. Chem. **51**, 129 (2000).

[16]W. C. Still, A. Tempczyk, R. C. Hawley, and T. Hendrickson, J. Am. Chem. Soc. **112**, 6127 (1990).

[17]N. A. Baker, Curr. Opin. Struct. Biol. **15**, 137 (2005).

[18]P. Ren, J. Chun, D. G. Thomas, M. J. Schnieders, M. Marucho, J. Zhang, and N. A. Baker, Q. Rev. Biophys. **45**, 427 (2012).

[19]K. Lum, D. Chandler, and J. D. Weeks, J. Phys. Chem. B **103**, 4570 (1999).

[20]D. Chandler, Nature (London) **437**, 640 (2005).

[21]R. Roth, Y. Harano, and M. Kinoshita, Phys. Rev. Lett. **97**, 078101 (2006).

[22]L. Wang, R. A. Friesner, and B. J. Berne, Faraday Discuss. **146**, 247 (2010).

[23]A. Ben-Naim, *Hydrophobic Interactions* (Plenum Press, 1980).

[24]C. Tanford, *The Hydrophobic Effect: Formation of Micelles and Biological Membranes* (John Wiley & Sons, 1980).

[25]J. Chen and C. L. Brooks III, J. Am. Chem. Soc. **129**, 2444 (2007).

[26]R. Zhou, X. Huang, C. J. Margulis, and B. J. Berne, Science **305**, 1605 (2004).

[27]B. J. Berne, J. D. Weeks, and R. Zhou, Annu. Rev. Phys. Chem. **60**, 85 (2009).

[28]J. Dzubiella, J. M. J. Swanson, and J. A. McCammon, Phys. Rev. Lett. **96**, 087802 (2006).

[29]J. Dzubiella, J. M. J. Swanson, and J. A. McCammon, J. Chem. Phys. **124**, 084905 (2006).

[30]L.-T. Cheng, J. Dzubiella, J. A. McCammon, and B. Li, J. Chem. Phys. **127**, 084503 (2007).

[31]L.-T. Cheng, Y. Xie, J. Dzubiella, J. A. McCammon, J. Che, and B. Li, J. Chem. Theory Comput. **5**, 257 (2009).

[32]L.-T. Cheng, Z. Wang, P. Setny, J. Dzubiella, B. Li, and J. A. McCammon, J. Chem. Phys. **131**, 144102 (2009).

[33]P. Setny, Z. Wang, L.-T. Cheng, B. Li, J. A. McCammon, and J. Dzubiella, Phys. Rev. Lett. **103**, 187801 (2009).

[34]L.-T. Cheng, B. Li, and Z. Wang, J. Comput. Phys. **229**, 8497 (2010).

[35]Z. Wang, J. Che, L.-T. Cheng, J. Dzubiella, B. Li, and J. A. McCammon, J. Chem. Theory Comput. **8**, 386 (2012).

[36]Z. Guo, B. Li, J. Dzubiella, L.-T. Cheng, J. A. McCammon, and J. Che, J. Chem. Theory Comput. **9**, 1778 (2013).

[37]J. Wang, S. Kudesia, D. Bratko, and A. Luzar, Phys. Chem. Chem. Phys. **13**, 19902 (2011).

[38]D. M. Anderson, G. B. McFadden, and A. A. Wheeler, Annu. Rev. Fluid Mech. **30**, 139 (1998).

[39]T. Biben, K. Kassner, and C. Misbah, Phys. Rev. E **72**, 041921 (2005).

[40]W. J. Boettinger, J. A. Warren, C. Beckermann, and A. Karma, Annu. Rev. Mater. Res. **32**, 163 (2002).

[41]L.-Q. Chen, Annu. Rev. Mater. Res. **32**, 113 (2002).

[42]Q. Du, C. Liu, and X. Wang, J. Comput. Phys. **198**, 450 (2004).

[43]J. B. Collins and H. Levine, Phys. Rev. B **31**, 6119 (1985).

[44]H. Emmerich, *The Diffuse Interface Approach in Materials Science: Thermodynamic Concepts and Applications of Phase-Field Models* (Springer, Berlin, 2003).

[45]G. H. Gilmer, W. Gilmore, J. Huang, and W. W. Webb, Phys. Rev. Lett. **14**, 491 (1965).

[46]L. Gránásy, J. Phys. Chem. **100**, 10768 (1995).

[47]D. Shao, W.-J. Rappel, and H. Levine, Phys. Rev. Lett. **105**, 108104 (2010).

[48]Y. Zhao, S. Das, and Q. Du, Phys. Rev. E **81**, 041919 (2010).

[49]Y. Zhao and Q. Du, Phys. Rev. E **84**, 011903 (2011).

[50]R. Petschek and H. Metiu, J. Chem. Phys. **79**, 3443 (1983).

[51]A. Karma and W. J. Rappel, Phys. Rev. E **60**, 3614 (1999).

[52]R. Benítez and L. Ramírez-Piscina, Phys. Rev. E **71**, 061603 (2005).

[53]B. Li and Y. Zhao, SIAM J. Appl. Math. **73**, 1 (2013).

[54]L. Modica, Arch. Ration. Mech. Anal. **98**, 123 (1987).

[55]P. Sternberg, Arch. Ration. Mech. Anal. **101**, 209 (1988).

[56]J. Chen, W. Im, and C. L. Brooks III, J. Am. Chem. Soc. **128**, 3728 (2006).

[57]N. Choudhury and B. M. Pettitt, J. Am. Chem. Soc. **127**, 3556 (2005).

[58]N. Choudhury and B. M. Pettitt, J. Am. Chem. Soc. **129**, 4847 (2007).

[59]J. A. Wagoner and N. A. Baker, Proc. Natl. Acad. Sci. U.S.A. **103**, 8331 (2006).

[60]J. Chen, C. L. Brooks III, and J. Khandogin, Curr. Opin. Struct. Biol. **18**, 140 (2008).

[61]P. W. Bates, Z. Chen, Y. H. Sun, G. W. Wei, and S. Zhao, J. Math. Biol. **59**, 193 (2009).

[62]Z. Chen, N. A. Baker, and G. W. Wei, J. Comput. Phys. **229**, 8231 (2010).

[63]R. C. Tolman, J. Chem. Phys. **17**, 333 (1949).

[64]L. Boruvka and A. W. Neumann, J. Chem. Phys. **66**, 5464 (1977).

[65]P.-M. König, R. Roth, and K. R. Mecke, Phys. Rev. Lett. **93**, 160601 (2004).

[66]Y. Marcus, J. Chem. Soc., Faraday Trans. **87**, 2995 (1991).

[67]D. Horinek, S. I. Mamatkulov, and R. R. Netz, J. Chem. Phys. **130**, 124507 (2009).

[68]T. Koishi, S. Yoo, K. Yasuoka, X. C. Zeng, T. Narumi, R. Susukita, A. Kawai, H. Furusawa, A. Suenaga, N. Okimoto, N. Futatsugi, and T. Ebisuzaki, Phys. Rev. Lett. **93**, 185701 (2004).

[69]A. P. Willard and D. Chandler, J. Phys. Chem. B **114**, 1954 (2010).

[70]J. Mittal and G. Hummer, Proc. Natl. Acad. Sci. U.S.A. **105**, 20130 (2008).

[71]F. Sedlmeier, D. Horinek, and R. R. Netz, Phys. Rev. Lett. **103**, 136102 (2009).